buildings

MDPI

Article

Study on Corrosion Fatigue Degradation Performance of Welded Top Plate-U Rib of Cross-Sea Steel Box Girder

Qian Cheng [1], Zhian Yao [2], Huanyong Chen [2,*], Dewei Liu [3], Mingyi Lin [3], Qiu Zhao [3] and Bin Zhang [1]

[1] CCCC Highway Bridges National Engineering Research Centre Co., Ltd., Beijing 100088, China; chengqian@bnerc.com (Q.C.); zhangbin@bnerc.com (B.Z.)
[2] Management Center of Shenzhen-Zhongshan Bridge, Zhongshan 528400, China; yaozhian@shenzhonglink.com
[3] College of Civil Engineering, Fuzhou University, Fuzhou 350108, China; 200520087@fzu.edu.cn (D.L.); 210520075@fzu.edu.cn (M.L.); zhaoqiu@fzu.edu.cn (Q.Z.)
* Correspondence: chenhuanyong@shenzhonglink.com

Abstract: With the development of the economy and transportation, more and more cross-sea bridges are appearing in people's view. However, cross-sea bridges are not only subjected to repeated traffic loads but also to corrosion from the marine environment. In addition, the steel box girder deck plate is directly subjected to repeated vehicle loads, and its welded details are highly susceptible to fatigue damage and destruction, resulting in fatigue or corrosion damage to the welded top plate-U rib of the cross-sea steel box girder. This paper is based on fracture mechanics analysis methods and finite element simulation analysis, in order to establish the numerical analysis method of the welded top plate-U rib of the steel box girder deck plate fatigue, which is to take into account the coupling of the marine corrosive environment and fatigue cyclic loading, explore the welded top plate-U rib of the stress intensity factor, crack expansion, crack expansion life and total fatigue life of the welded details. Furthermore, the establishment of the welded top plate-U rib corrosion fatigue life assessment model is to explore the fatigue life of different top plate thicknesses. The results show that: the stress intensity factor along the crack front is symmetrically distributed, and with the increase in the crack expansion step, the corresponding stress intensity factor amplitude is also increasing; in addition, with the increase in the top plate thickness, fatigue crack expansion rate significantly reduced.

Keywords: cross-sea bridge; steel box girder; welded; top plate-U rib; corrosion fatigue; crack expansion; fatigue life

check for updates

Citation: Cheng, Q.; Yao, Z.; Chen, H.; Liu, D.; Lin, M.; Zhao, Q.; Zhang, B. Study on Corrosion Fatigue Degradation Performance of Welded Top Plate-U Rib of Cross-Sea Steel Box Girder. *Buildings* **2023**, *13*, 1784. https://doi.org/10.3390/buildings13071784

Academic Editors: T. Tafsirojjaman, Yue Liu and Scott T Smith

Received: 28 May 2023
Revised: 19 June 2023
Accepted: 4 July 2023
Published: 13 July 2023

1. Introduction

With the development of the economy and transportation, cross-sea bridges becoming more and more widespread. The construction of large cross-sea bridges, such as the Hong Kong-Zhuhai-Macao Bridge, the Jiaozhou Bay Cross-Sea Bridge, and the Pingtan Strait Road-Rail Bridge, etc., plays a pivotal role in realizing the interconnection of economic regions along the "the Silk Road Economic Belt and the 21st-Century Maritime Silk Road". However, the cross-sea bridge should not only bear the action of structural self-weight and traffic loads but also bear the challenge of a marine corrosive environment on the durability of the bridge structure. The steel box girder, which has the advantages of being lightweight, having large bearing capacity, good wind resistance stability, and large torsional stiffness, is mostly used in the cross-sea bridge. It can be prefabricated in the factory and assembled on the construction site, greatly shortening the construction period. Furthermore, steel box girders commonly use orthotropic steel bridge decks, which have the benefits of lightweight, high strength, and factory production and are frequently used in bridge structural design. However, its structure is complex and has a large number of long welds. In addition, the structure itself has a lot of defects and its construction quality cannot be fully guaranteed, resulting in the bridges—which use orthotropic steel bridge decks—easily forming fatigue damage.

At present, the research on steel box girder corrosion or fatigue by scholars at home and abroad is becoming more and more mature. Kayser et al. [1] established a corrosion deterioration model by combining corrosion location and corrosion rate with the structural analysis method and explored the influence of corrosion on steel beams by evaluating the residual bearing capacity of bending stress and shear failure. Cui et al. [2] took a typical orthotropic steel bridge deck of an urban overpass as the research object and used the extrapolation method recommended by the International Institute of Welding (IIW) [3] to calculate the hot spot stress spectrum of its key vulnerable parts, and calculated its life through the hot spot stress S-N line and linear cumulative damage theory. Zhang et al. [4] used the steel box girder of the Hong Kong-Zhuhai-Macao Bridge as the research object and conducted fatigue test research on several key fatigue-prone parts with the full-scale segmental model, The study showed that the fatigue performance of the orthotropic steel bridge panels of the Hong Kong-Zhuhai-Macao Bridge met the design requirements and had certain safety reserves. Meng [5] explored the effects of finite element cell type, corrosion pit shape, corrosion pit distribution, corrosion pit depth, and corrosion volume loss on the ultimate strength of stiffened plates through the calculation model of the ultimate strength of stiffened plates with pitting corrosion. The results indicated that corrosion volume loss was the main influencing factor on the ultimate strength of stiffened plates with pitting corrosion. Zhong [6] summarized the typical diseases of large-span suspension steel box girders, the connection welds of steel bridge panel components are the weak parts of steel box girders, which are easy to produce fatigue cracks under alternating loads. And corrosion usually occurs in the inner wall of steel box girders, which will reduce the effective area of steel box girders and decrease their service life. Zhong Xin [7] analyzed the steel box girder structure under the repeated load of vehicles. The research showed that the U-rib and diaphragm of steel box girder were prone to fatigue damage and predicted the subsequent development of fatigue cracks in steel box girder. Finally, the countermeasures to alleviate the development of cracks in the steel box girder were put forward. Zhou et al. [8] investigated the fatigue characteristics of typical vulnerable parts of orthotropic anisotropic steel bridge panels by fatigue tests with foot-rule models. The study showed that the hot spot stress method and the notched stress method had better evaluation results than the nominal stress method. Wei et al. [9] explored the corrosion fatigue performance of welded joints of steel structure bridges. It was found that there was a significant interaction between the factors affecting corrosion. At present, the corrosion fatigue crack propagation models are mainly the superposition model, product model, and competition model. Zhang [10] explored the stress mechanism of ribbed stiffened plates under three conditions: local stability, overall stability, and local-global coupling stability under compression through compression tests and finite element methods, and proposed a calculation method for the local stability reduction coefficient and overall stability reduction coefficient of ribbed stiffened plates. Zhao et al. [11–13] conducted overall and local stability performance tests on U-rib stiffeners to study the buckling performance of U-rib and each component plate, which showed that with the increase of web or stiffened plate width to thickness ratio, the damage mode of the specimen gradually changed from strength damage to instability damage, and the characteristics of instability damage was also more obvious.

However, there are few studies on the fatigue damage of steel box girders under the combined action of corrosion and fatigue. In this paper, the details of the top plate-U rib weld of the steel box girder bridge deck were taken as the research object. Considering the coupling effect of marine corrosion environment and fatigue load, the fatigue damage behavior and corresponding fatigue failure mechanism of the top plate-U rib welded details of the steel box girder bridge deck were studied by numerical simulation method. The degradation law of mechanical properties of the top plate-U rib welded steel box girder in a corrosive environment was revealed, and then the fatigue life was predicted.

2. Materials and Methods

2.1. Fracture Mechanics Fatigue Analysis Methods

The fracture mechanics method is based on the size of the crack and the crack extension rate as the basis of fatigue analysis. The method defines the critical length of fatigue cracks and establishes the theoretical model of fatigue crack extension. Its underlying theory, the Paris formula (as in Equation (1)), and the extension approach based on the Paris formula have yielded beneficial results in the domains of fatigue performance analysis, remaining life prediction, and normal service maintenance of orthotropic anisotropic steel bridge panels. Meanwhile, in recent years, researchers have successfully combined the fracture mechanics method with finite elements to realize the parametric simulation of the crack extension process, which clearly recognizes the fatigue-dominated cracking and ex-tension modes of fatigue details of orthotropic anisotropic steel bridge panels and has become a very effective method to study the fatigue development and structural de-gradation mechanism of orthotropic steel bridge panels.

$$\frac{da}{dN} = C\left(\Delta K_{eff}\right)^{n} \tag{1}$$

where a is the crack propagation depth, N is the number of load cycles, C and n are material-related coefficients, ΔK_{eff} is the stress intensity factor amplitude at the crack tip. In the theory of fracture mechanics, the equivalent stress intensity factor K_{eff} is usually used to judge the characteristics of the crack front edge. And according to the calculation formula recommended in BS7910 [14]:

$$K_{eff} = \sqrt{K_I^2 + K_{II}^2 + \frac{K_{III}^2}{1-v}} \tag{2}$$

where K_I, K_{II}, K_{III} are the crack stress intensity factors corresponding to the three cracking modes of type I, type II, and type III, respectively, ν is the Poisson's ratio of the material. According to the stress intensity factor criterion of linear elastic fracture mechanics (LEFM) to determine whether the crack continues to expand, the crack expansion criterion is:

$$K_{eff} \geq K_{th} \tag{3}$$

where K_{th} is the fatigue crack stress intensity factor expansion threshold of the material. According to the current research results in fracture mechanics, when the crack leading edge of the equivalent stress intensity factor K_{eff} is greater than the material fatigue cracking stress intensity factor threshold K_{th}, the crack will continue to expand. Fatigue cracks appearing at the welded details are located in the weld influence region. Referring to BS7910, this paper's fatigue crack stress intensity factor expansion threshold recommended value is K_{th} = 2 MPa·m$^{1/2}$.

2.2. Time-Varying Model of Marine Corrosion

According to the specification GB/T 15957-1995 "Atmospheric Environment Corrosion Classification" [15], the components of the atmospheric environment are divided into four types of atmospheric environment: rural environment, urban environment, industrial environment, and marine environment, which the industrial environment and marine environment are atmospheric environments with high corrosiveness. In the marine atmosphere, the evaporation of Cl- from seawater is the main cause of steel corrosion, and when a large amount of Cl− dissolves in the water film on the steel surface [16]. It enhances the electrical conductivity of the water film, and at the same time accelerates the polarization reaction of steel, which leads to an increase in the corrosion rate of steel.

The accuracy and feasibility of civil and structural engineering quality analysis depend to some extent on the quality of the model, and a simple and accurate corrosion time-varying model can make the corrosion coupling model more realistic. Liang et al. [17] carried out a 16-year open-air corrosion test of 17 types of steel in the atmospheric environment, obtained the atmospheric corrosion test data from seven test points and found that the corrosion law of steel basically follows the power exponential model. Therefore, the power exponential model is used as the base model of the corrosion time variation law in this paper, and the base formula of the power exponential model is shown in Equations (4)–(6):

$$D = At^n \tag{4}$$

$$A = A_0 + A_{(i)}Y_{(i)} \tag{5}$$

$$n = n_0 + n_{(i)}Y_{(i)} \tag{6}$$

where D is the corrosion depth of steel (mm), t is the exposure time of steel in the environment (years), A_0 and n_0 are constants, A_0 = 0.031, n_0 = −0.079; $A_{(i)}$ and $n_{(i)}$ are factors of factor i; $Y_{(i)}$ is the number of factor i. When the factor is the chemical composition of the steel, $Y_{(i)}$ is the percentage content of the chemical composition of the steel. When the factor is the environmental factor, $Y_{(i)}$ is the average or cumulative amount of the environmental factor, such as the average temperature. The coefficient values of each influencing factor are shown in Table 1.

Table 1. Influence factor coefficient value.

Influence Factor	Units	Coefficient n	Coefficient A	Remarks
Constant term	-	−0.079	0.031	
Relative humidity	%/100	0.216	-	Annual mean
Temperature	°C/100	-	0.367	Annual mean
Chlorate ion	mg/(100 cm^2·d)	1.022	0.016	Rate of deposition
Sulfur dioxide	mg/(100 cm^2·d)	0.195	0.028	Rate of deposition
Rainfall times sunshine hours	(mm/a)·(h/a)·10^{-6}	0.145	−0.021	Annual total
Copper	%	−0.452	-	Content in steel
Manganese	%	-	−0.013	Content in steel
Silicon	%	0.052	−0.022	Content in steel
Phosphorus	%·10	−0.069	−0.024	Content in steel
Sulfur	%·10	0.375	0.036	Content in steel

In this paper, the stiffening girder of a coastal cable-stayed bridge is taken as the research object. After investigation, the average annual temperature in the area is 22.7 °C, the average relative humidity is 79%, the annual sunshine time is 1641.7 h, the average annual rainfall is 1890 mm, the average sulfur dioxide content is 0.107 mg/(100 cm^2·d), the chloride ion content is 0.024 mg/(100 cm^2·d). The commonly used Q345D steel is taken as an example, and the chemical composition content is based on the standard GB/T 1591-2018 “low-alloy high-strength structural steel” [18].

Some of the chemical composition content in standard for the range of values. To obtain a more unfavorable corrosion model, the content of elements conducive to the corrosion of steel to take the maximum value, and the content of elements unfavorable to the corrosion of steel to take the average or minimum value. Therefore, it can be calculated to obtain the initial corrosion rate of the coastal sea area A = 0.0643, corrosion rate change trend n = 0.7559, to obtain the predicted relationship between corrosion depth and time in the coastal area is as in Equation (7):

$$D = 0.0643t^{0.7559} \tag{7}$$

Since the steel box is in a more closed state for a long time, the influence of the marine environment is weak, the corrosion of steel inside the steel box is not considered for the time being in the analysis, and the focus is the corrosion on the top side of the steel box beam.

2.3. Corrosion Model of Welded Details

The corrosion fatigue effect of steel bridges is the result of the long-term interaction between the corrosive marine environment and cyclic traffic loads on steel bridges. As illustrated in Figure 1, the electrochemical effects of the corrosive environment cause microstructural changes in the steel and crack surfaces in the early stages of corrosion fatigue, including steel oxidation, changes in the composition of the chemical elements of steel, and changes in grain size.

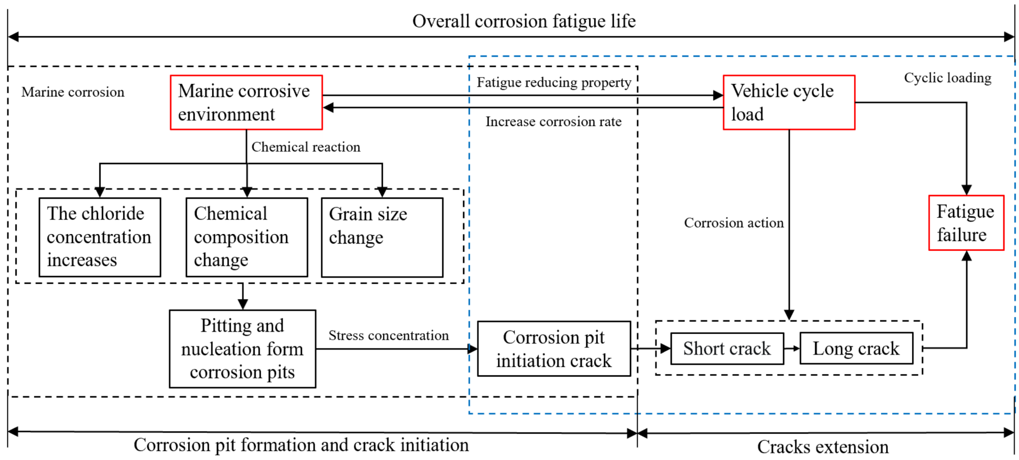

Figure 1. The mechanism of corrosion fatigue action.

In addition, due to the large number of chloride ions in the marine atmospheric environment and the cyclic effect of traffic loading, it is very easy to induce localized corrosion or pitting, resulting in pitting nucleation.

Stress concentration is formed at the pitting pits and cracks are gradually generated inside the corrosion pits. The cracks are more likely to be corroded by the environment, which increases the corrosion degree and accelerates the rate of crack expansion.

There are two main reasons for etch pit nucleation: passivation film damage theory and adsorption theory. Theoretically, the etch nucleation can be randomly formed at any place on the metal surface, but when the passivation film has local defects, sulfide inclusions inside, and carbide deposition on the grain boundary, the etch nucleation will be preferentially formed at these points. Pitting corrosion is a form of corrosion in which holes or pitting appear on the metal surface in a small range in some corrosive media and continue to develop in-depth to form small holes. The pitting morphology varies with different materials and corrosive media, showing an irregular shape, as shown in Figure 2. However, pitting pits are generally simplified into hemispherical, semi-ellipsoidal, conical, and cylindrical in the finite element simulation.

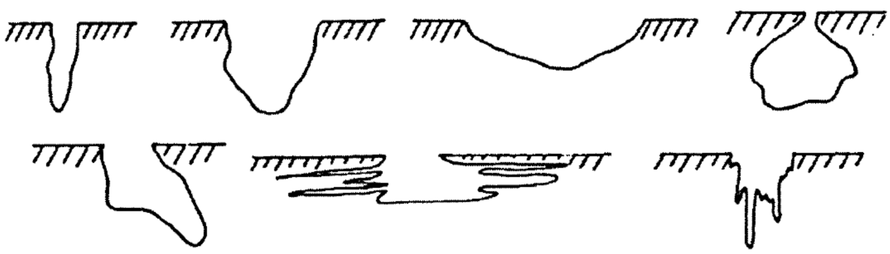

Figure 2. Various pitting morphologies.

Pitting corrosion is easy to occur in steel structure bridges in marine atmospheric environments, and the damage caused by pitting corrosion is much more serious than that of uniform corrosion, which is mainly manifested by large stress concentrations near the corrosion pit. The effect of corrosion on the welding area is mainly to change the stress distribution, which affects the fatigue life of the welded joint. To better study the influence of pitting corrosion on welded fatigue details, the hemispherical shape is used as the simplified shape of the finite element model of the corrosion pit, and the corrosion depth (D) is used as the radius of the spherical corrosion pit (R). According to the prediction relationship between corrosion depth and time in the coastal area of Guangzhou, it can be obtained:

$$R = D = 0.0643t^{0.7559} \tag{8}$$

where R is the radius of the artificial spherical pit (mm); D is the corrosion depth of steel (mm); t is the exposure time of steel in the atmosphere (years).

The connection of the top plate-U rib welded is mostly a single-sided fillet weld, although the proportion of such welds in fatigue-prone parts is only about 20%. However, the key fatigue failure mode of this part is that the fatigue crack appears at the welding root or toe of the top plate and spreads along the direction of the top plate, so it is difficult to inspect and detect the crack at the early stage of development. Generally, only when the fatigue crack develops to a certain length, or cracks have even come through the top plate leading to the waterproof layer of the bridge panel and pavement can damage be found, often at this time a lot of rain has infiltrated into the fatigue damage parts into the longitudinal rib or steel box girder, and the fatigue cracking repair work of the parts is more difficult, generally need to interrupt traffic, It is the most serious fatigue crack of orthotropic steel bridge panel. However, the key fatigue failure mode of this part is that the fatigue crack appears at the welding root or toe of the top plate and spreads along the direction of the top plate, so it is difficult to inspect and detect the crack at the early stage of development. Generally, it can be found only when the fatigue crack develops to a certain length, or even when cracks have come through the top plate leading to the waterproof layer of the bridge panel and pavement damage. At this time, a lot of rain has infiltrated the fatigue damage parts into the longitudinal rib or steel box girder, and the fatigue cracking repair work of the parts is more difficult. It is the most serious fatigue crack of the orthotropic steel bridge panel.

The cracking modes of the top plate-U rib weld are as follows: first, the toe cracks along the top plate; second, The welding root cracking along the top plate; third, Weld toe cracking along the U rib; fourth, The welding root cracks along the weld.

As the interior of the steel box girder is relatively closed, the external environment has less influence on the interior of the box girder, and the corrosion inside the box girder is relatively light, mainly the corrosion of the outside of the box girder. The cracking modes with greater corrosion influence are toe cracking along the top plate and root cracking along the top plate, so the spherical pit corrosion is set on the outside of the top plate directly above the weld toe and the weld root, as shown in Figure 3.

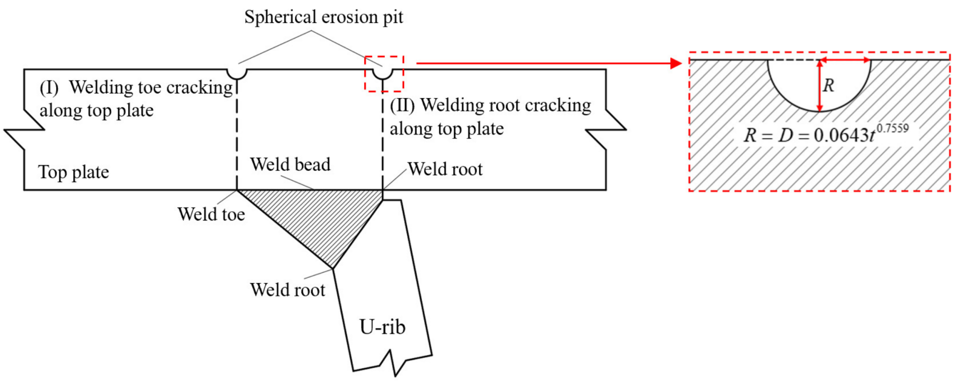

Figure 3. Corrosion-influenced cracking patterns and spherical pits.

3. Finite Element Model

3.1. The Finite Element Model Considering Corrosion State

The finite element software ABAQUS 6.14 was used to establish the welded fatigue details model of the top plate-U rib under corrosion conditions. The roof and U rib were connected by 80% penetration welds, as shown in Figure 4.

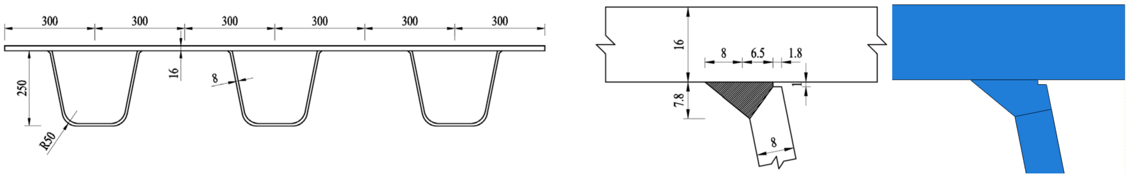

(**a**) (**b**)

Figure 4. Steel bridge panel construction details dimensions: (**a**) U-rib structure details; (**b**) Weld construction details.

The top plate and U-rib sections were constructed using hexahedral solid cells (C3D8R) in ABAQUS, with an encrypted cell mesh in the area of concern for spherical erosion pits in the top plate-U-rib weld. Q345qD steel was used with a modulus of elasticity of 2.06×10^5 MPa and a Poisson's ratio of 0.3. The weld and fusion zone properties are consistent with the parent material. The wheel position has a small transverse influence on the U-rib weld of the steel bridge panel, with the U-rib weld near the top plate affecting about 900 mm and the other parts affecting about 600 mm. Therefore, the transverse width of the local model of the U-rib of the simulated steel bridge panel is 1800 mm, which includes three U-ribs, and the longitudinal width is 200 mm.

The boundary conditions were set to constrain the vertical and lateral translational degrees of freedom and rotational degrees of freedom on both sides of the bottom of the U-rib. Fixed constraints were set at both ends of the top plate. The finite element model and boundary settings are shown in Figure 5.

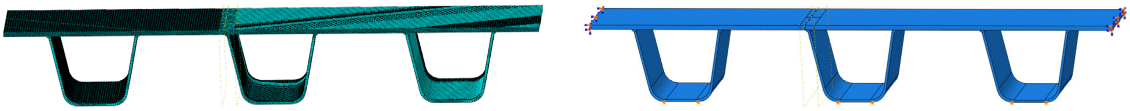

(**a**) (**b**)

Figure 5. Model meshing and boundary condition setting: (**a**) Model meshing; (**b**) Boundary condition setting.

The top plate-U-rib weld construction detail on the left side of the second U-rib was selected as the object of corrosion fatigue detail analysis.

Based on the corrosion pit simulation method, the symmetry of the structure was considered to reduce the influence of model boundary conditions on the corrosion pit. The depth of the corrosion pit was set at 1.24 mm (50 years of corrosion). The implant position was set at 100 mm of the longitudinal centerline coordinate, and the transverse coordinates are directly above the weld toe or weld root line, as shown in Figure 6. Then the top plate-U rib finite element models of cracked modes (I), cracked modes (II), and both cracking modes were established respectively.

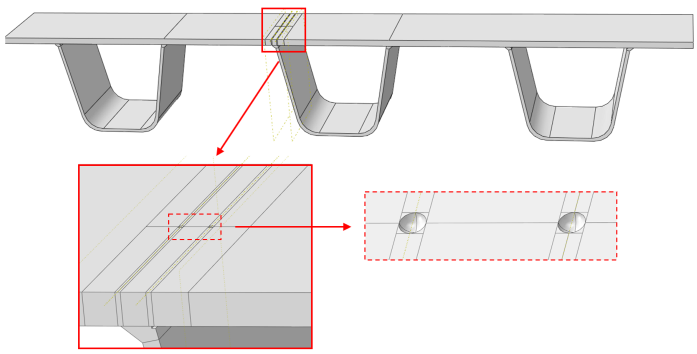

Figure 6. Finite element model of top plate-U rib with corrosion pits.

3.2. Fatigue Loading

According to the specification JTGD64-2015 "Design Code for Highway Steel Bridges" [19], the bridge deck system members were verified using fatigue load calculation model III with a vehicle weight of 480 kN, and their axle loads, and distribution are shown in Figure 7. The peak principal stresses caused by the uniaxial action and the multi-axial action correspond to the same peak value. The literature study shows that the diffusion effect in the wheel load area of the deck pavement was not considered in the stress analysis of the top plate-U rib weld of the deck slab. A double wheel loading was used with a wheel load distribution area of 200 mm × 600 mm and the wheel load was located above the top plate-U rib weld in the relevant area of the foundation pit. The loading conditions are shown in Figure 8.

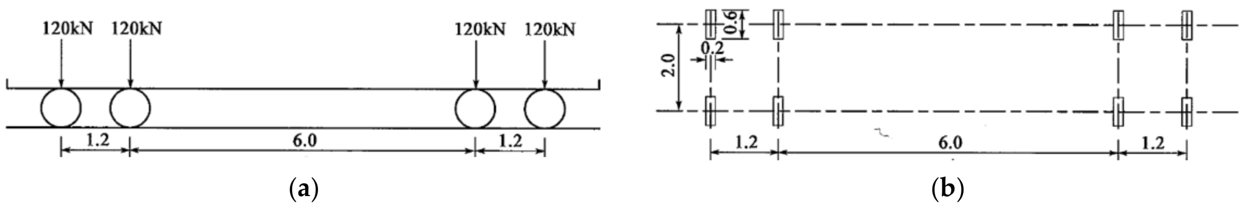

Figure 7. Fatigue load model III: (**a**) Elevation view of load layout; (**b**) Plan view of load. layout.

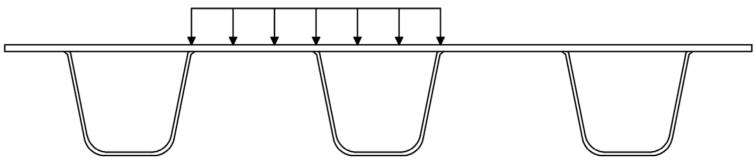

Figure 8. Finite element model of loading.

3.3. Implantation of Fatigue Cracks

The FRANC3D 7.5.5 software was used to establish the relationship between the defect and the fatigue performance of the component by implanting the initial crack defect at a specified location, tracking and calculating key information such as step length, expansion angle, stress intensity factor, and fatigue life of each crack expansion step.

The initial defect implantation process starts by importing the complete top plate-U rib finite element model created in ABAQUS into the FRANC3D program to divide the sub-model and implant the initial fatigue at the mid-point of the bottom of the corrosion pit in the top plate of the sub-model, as shown in Figure 9.

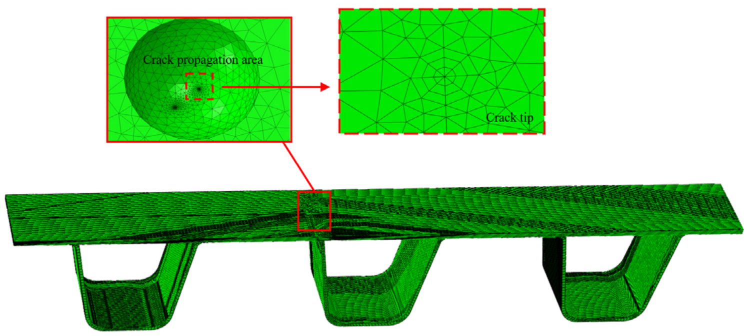

Figure 9. Crack implantation in ABAQUS.

The International Institute of Welding (IIW) recommends that the surface cracks were characterized by semi-elliptical defects, with a0 denoting the short semi-axis length and c0 denoting the long semi-axis length. The FRANC3D program implants the crack-tip singular unit rings by redividing the sub-model cells. In this case, the innermost part is a quarter-node wedge cell, and the outer part is a second-order hexahedral cell ring, as shown in Figure 10. After implanting the cracks, the ABAQUS solver was called to carry out the calculation and analysis, and the stress intensity factor at the crack tip is calculated by reading the "odb" file in ABAQUS, and then the initial crack was updated by defining the expansion step and the relevant parameters of the fatigue crack expansion criterion; then the ABAQUS solver was called again to carry out the cycle is repeated until the fatigue damage of the structure is reached.

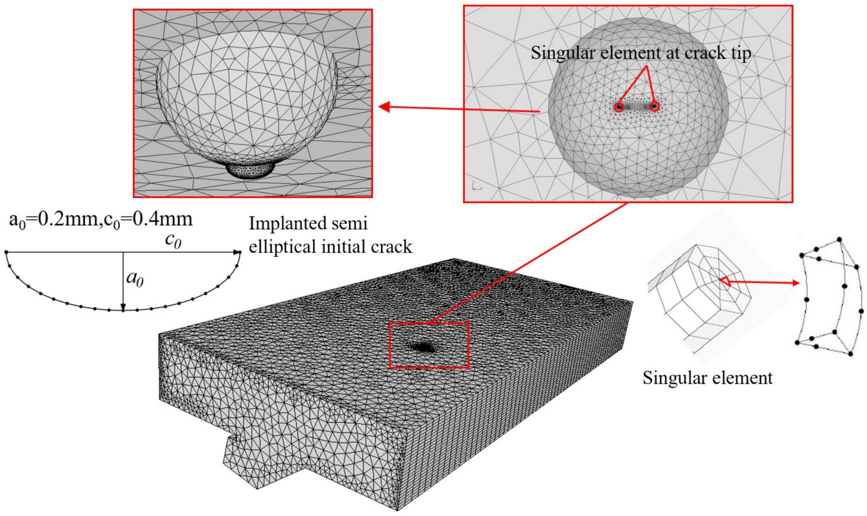

Figure 10. FRANC sub-model and crack implantation.

According to IIW, the recommended steel crack growth parameters are $C = 1.65 \times 10^{-11}$ MPa·m$^{1/2}$, m = 3, and threshold value K_{th} = 2 MPa·m$^{1/2}$. The crack propagation parameters of steel will change due to the coupling effect of corrosion and fatigue. Considering the accuracy and operability of the model calculation, for the model with corrosion, the crack expansion parameter is taken as $C = 2.21 \times 10^{-11}$ MPa·m$^{1/2}$, m = 3, threshold value K_{th} = 1.5 MPa·m$^{1/2}$, and the crack expansion parameter for the model without corrosion is taken as the recommended value of IIW. BS7910 recommends that the short semi-axis of the initial defect is 0.1–0.5 mm, while the initial defect shape ratio is usually taken as 0.2–0.5, in order to ensure smooth crack expansion and minimize the impact of the initial crack on the total life of the crack expansion, take the smaller value of a_0 = 0.2 mm, c_0 = 0.4 mm, that is, the defect shape ratio a_0/c_0 is 0.5, and designated as the benchmark initial defect size. It is conservative to develop a critical damage value of 1/2 of the top plate thickness, that is, 8 mm.

4. Stress Intensity Factor and Crack Growth Analysis

4.1. Stress Intensity Factor Analysis

The stress intensity factor of fatigue detail crack propagation under corrosion conditions is calculated and analyzed. The cracked modes(I) were used to make finite element analyses. The corrosion life of 0 years and 50 years (i.e., no corrosion and corrosion pit radius R = 1.24 mm).

The models were named *a*-000 and *a*-050, and the semi-elliptical shape was taken as the initial crack of crack growth. In order to minimize the impact of the initial crack on the total crack life, the size was taken as short semi-axial value a_0 = 0.2 mm and long semi-axial value c_0 = 0.4 mm, that is, the defect shape ratio a_0/c_0 = 0.5. The crack was implanted in the center of the bottom of the pit perpendicular to the top plate, as shown in Figure 11. Firstly, the weld and the nearby part of the top plate were defined as sub-models with a transverse width of 50 mm and a total length of 200 mm in the longitudinal direction. Then the initial crack was implanted at the bottom of the pit. In order to consider the calculation accuracy and efficiency, when the crack width was less than the width of the pit, the crack growth step was 0.01–0.1 mm, when the crack width was larger than the etch pit width, the crack growth step was 0.1–0.5 mm. In order to ensure smooth crack growth, the specific value was determined by the actual situation. The ring radius of the crack tip was about 15% of the total length of the current crack growth, that is when the total length of the crack growth was 2 mm, the ring radius of the crack tip was 0.3 mm.

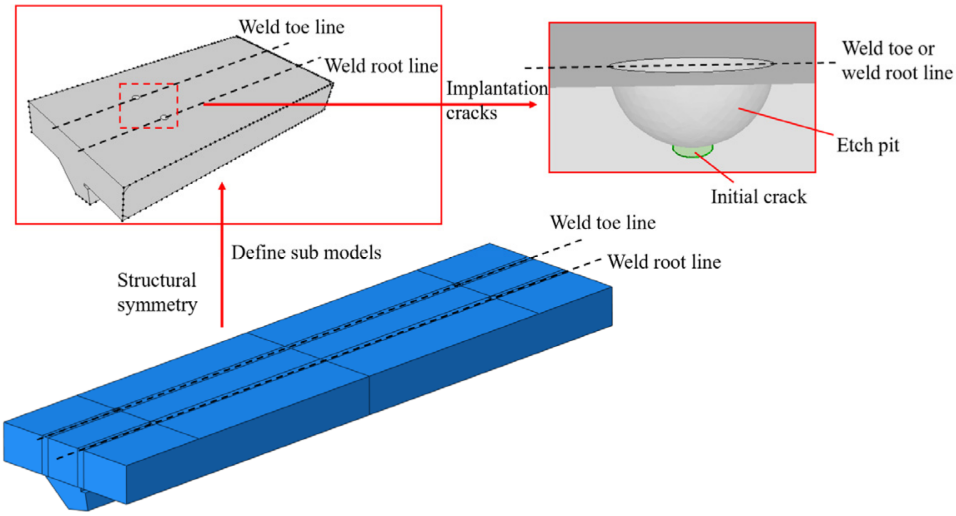

Figure 11. Initial crack implantation.

The fatigue crack expansion history in the presence of pit corrosion can be broadly divided into three processes [20–22]: crack expansion inside the pit (referred to as internal cracking), crack expansion across the edge of the pit, and crack expansion outside the pit (referred to as external cracking), as shown in Figure 12. Each elliptical arc in the diagram represented the pattern of crack expansion, and the distance between the two lines was the step length of each crack expansion step.

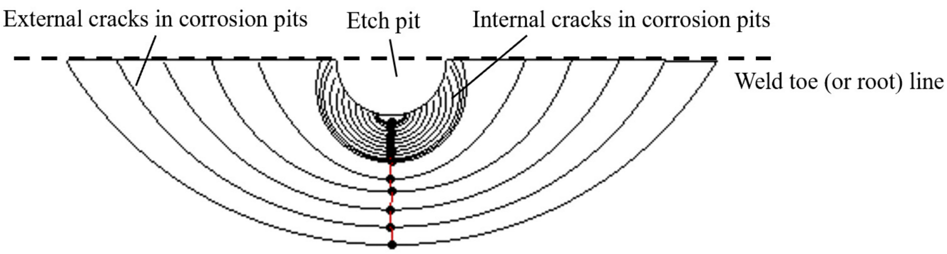

Figure 12. Crack extension pattern.

To clearly understand the variation pattern, the stress intensity factor curves of the crack tip corresponding to the 1st, 5th, 10th, 11th, 20th, and 29th extension steps of model *a*-050 were extracted as shown in Figure 13, where the 10th and 11th extension steps were the last and the first extension steps before and after the crack crosses the etch pit. The stress intensity factor was symmetrically distributed along the crack front, the stress intensity factor of the first extension step showed a trend of decreasing and then increasing, with the maximum value obtained at the two endpoints and the middle. As the crack extension step increases, the corresponding stress intensity factor amplitude also increased, and the stress intensity factor amplitude ΔK_{eff} on both sides of the crack near the end increased more than that at the middle point. When the crack crosses the pit, the stress intensity factor ΔK_{eff} increased to 1.49 times the original value at both ends of the crack front, while the increase near the mid-point was smaller.

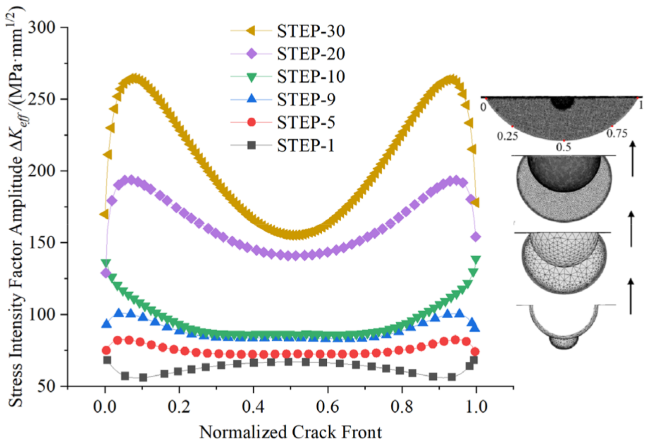

Figure 13. Stress intensity factor amplitude distribution.

In order to study the effect of etch pit size on crack extension, crack extension analysis was carried out for the finite element model with and without corrosion, and the variation curve of crack leading edge depth a_1 and crack leading edge equivalent strength factor amplitude ΔK_{eff} was obtained. *a*-050 model crack leading edge end (position 0) and crack leading edge midpoint position (position 0.5) were compared with a_1-ΔK_{eff} curve of *a*-000 model The comparison analysis is shown in Figure 14, where the crack leading edge depth a_1 was the sum of the etch pit depth R and the crack extension depth a. From the Paris formula, it can be seen that ΔK_{eff} is positively correlated with the crack extension rate da/dN.

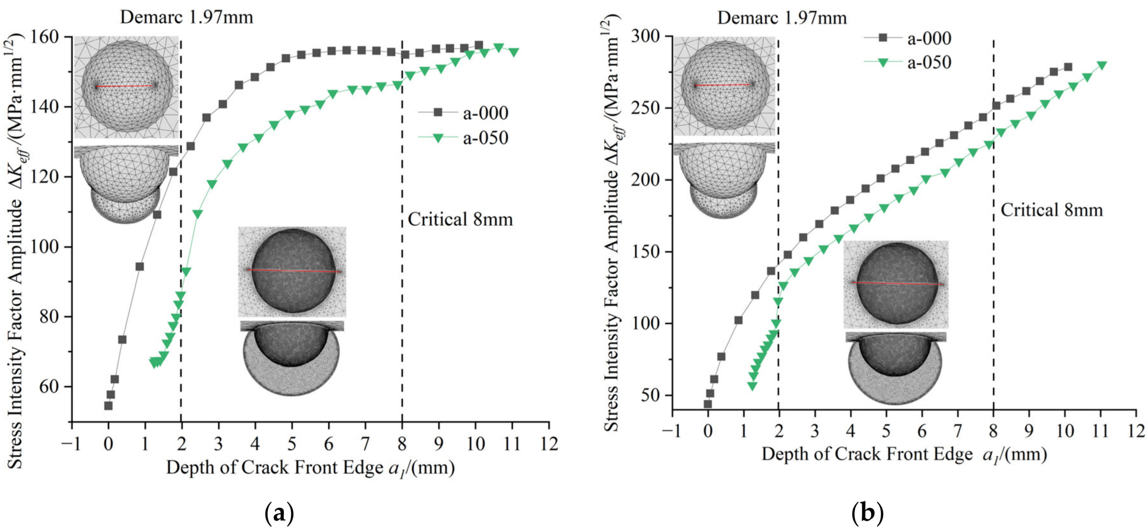

Figure 14. a_1-ΔK_{eff} curves for models at different positions: (**a**) a_1-ΔK_{eff} curve at position 0; (**b**) a_1-ΔK_{eff} curve at position 0.5.

As can be seen from Figure 14a, it can be seen that the slope of the *a*-000 model curve at position 0 decreases first and then remains basically unchanged with crack growth. The slope of the *a*-050 model curve showed a gradual decrease-surge-decrease with crack expansion and then was fundamentally the same as the *a*-000 model. When the crack expands inside the etch pits, that is, the crack leading edge depth was less than the cut-off points of 1.92 mm (where the pit depth was 1.24 mm and the crack extension depth was 0.68 mm). The ΔK_{eff} of the *a*-000 model was greater than that of the *a*-050 model at the same crack leading edge depth, corresponding to a faster crack extension rate da/dN. When the crack leading edge was about to cross the cut-off point, the slope of the *a*-050 model curve increased rapidly, leading to a sharp increase in ΔK_{eff}, and the difference with the

a-000 model decreased after crossing the cut-off point. The slope of the a-050 model curve converged with that of the a-000 model when the crack crossed the cut-off point.

As can be seen from Figure 14b, the slope of both the a-000 and the a-050 model curve at position 0.5 showed a trend of gradually decreasing with crack expansion. When the crack expanded inside the pit, the crack leading edge depth was less than the parting point of 1.92 mm, the two curves changed at similar rates, and the ΔK_{eff} of the a-000 model was greater than that of the a-050 model at the same crack leading edge depth, corresponding to a faster crack expansion rate da/dN. The slope of the a-050 model curve was greater than the slope of the a-000 model curve when the crack crossed the cut-off point and extends outside the pit, and the stress intensity factor of the a-050 model tended to exceed that of the a-000 model.

Comparing the a_1-ΔK_{eff} curves at position 0 and position 0.5 of the a-050 model, we could see that the influence of the pit on ΔK_{eff} at position 0 was concentrated in the process of crack expansion inside the etch pit and crack crossing the etch pit. When the crack crossed the pit, the pit erosion had little effect on it. The influence of the crater on ΔK_{eff} at position 0.5 was mainly the process of crack propagation outside the crater, and when the crack crosses the crater, the influence of the crater decreased gradually with the crack propagation. When the crack crosses the etch pit, the influence of the pit on ΔK_{eff} at position 0.5 was mainly in the process of crack expansion outside the etch pit, and when the crack crosses the etch pit, the influence of the pit on ΔK_{eff} decreased as the crack expands. The influence of the pit on ΔK_{eff} at location 0.5 is mainly due to the expansion of the crack outside the pit. As the crack crosses the pit, the influence of the pit on it decreased as the crack expands.

4.2. Dynamic Analysis of Crack Growth

To study the crack extension morphology, and the crack extension life with the crack depth change law, we established the corrosion model of fatigue crack extension history, as shown in Figure 15. It could be found that as the crack expanded, its morphology gradually evolved from the initial semi-ellipse to a close semi-circle, and finally gradually evolved to a flat semi-ellipse.

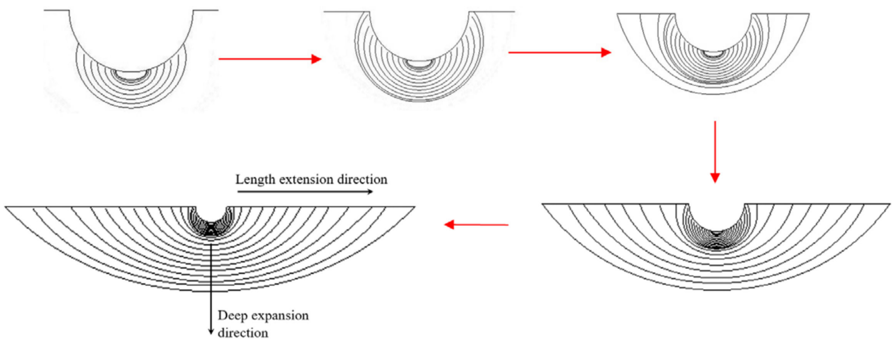

Figure 15. Fatigue crack expansion history.

The shape ratio of the a-050 corrosion model and a-000 corrosion-free model during the crack expansion process is shown in Figure 16. The trends of the curves of the two models are similar. For the a-000 model, as the crack extension depth increased, the shape ratio of the crack showed a tendency to increase rapidly to a maximum value and then decreased linearly, with a maximum value of about 0.82. For the a-050 model, when the leading edge of the crack did not cross the dividing point, as the crack extension depth increased, the shape ratio of the crack showed a tendency to increase rapidly to a maximum value and then decreased, with a maximum value of about 0.70. As the leading edge of the crack crossed the demarcation point, the shape ratio decreased at a slower rate than the a-000 model and nearly was linear and will intersect the a-000 model curve as the crack extends to 11 mm.

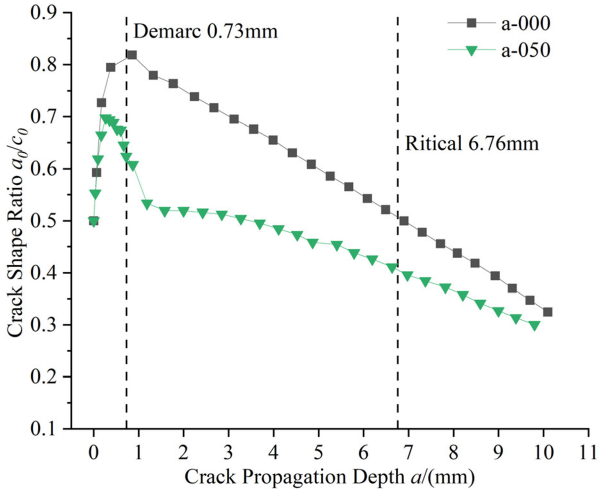

Figure 16. Crack shape ratio change curve.

The cracking *a*-*N* curves for the corroded and uncorroded models are shown in Figure 17. The trend of fatigue life change for both models showed a slow and then accelerated trend, with the *a*-050 corrosion model having a faster fatigue life change rate than the *a*-000 corrosion model. When the crack leading edge depth a_1 reached the critical value (half of the top plate thickness, 8.0 mm, where the crack of the *a*-050 model extends by 6.76 mm and the *a*-000 model extends by 8 mm), the fatigue life of the *a*-050 model is 9.55 million cycles and that of the *a*-000 model is 12.394 million cycles; when the crack of the *a*-050 model extends by 8 mm The fatigue life is 10.208 million cycles when the crack of the *a*-050 model extends by 8 mm, which corresponds to a crack leading edge depth of 9.24 mm.

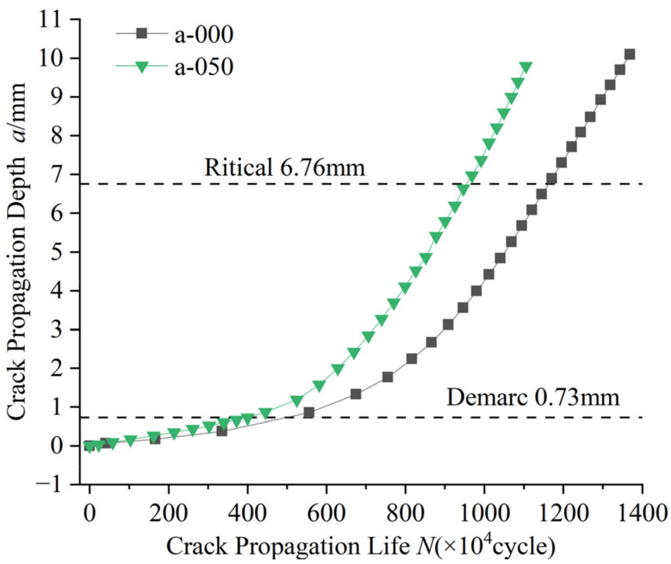

Figure 17. *a*-*N* curves graph.

5. Top Plate–U Rib Welded Detail Corrosion Fatigue Life Assessment Model

5.1. Corrosion Fatigue Life Assessment Model

At present, the life assessment of corrosion fatigue of steel structures in the marine environment can generally be simplified into two stages: the initial stage is dominated by corrosion and the later stage by structural fatigue damage. In this paper, the corrosion fatigue action of steel beams was divided into two stages: the pitting stage and the crack expansion stage. The pitting stage was dominated by the corrosive environment, while the crack extension stage was dominated by the cyclic action of the bridge traffic load, which included the short crack extension stage and the long crack extension stage. The expression for the fatigue life of a steel bridge structure in a corrosive environment is

$$T = T_1 + T_2 \tag{9}$$

where T is the total corrosion fatigue life of the steel bridge, T_1 is welded detail etch pit generation and expansion time, T_2 is the time from fatigue crack expansion to welded detail failure (including short crack and long crack expansion time).

Marine corrosion environment steel bridge structure pitting corrosion pit formation was the first step of the steel structure corrosion fatigue damage. According to the formula (7) of the prediction of the relationship between corrosion depth and time in the coastal area of Guangzhou City, the corrosion pit depth D with time was acquired. The crack sprouting expansion rate was greater than the corrosion pit corrosion expansion rate, so after the sprouting of cracks, the crack expansion was regarded as the main structural failure mode. The corrosion years of 10, 30, 50, 80, and 100 years and the corrosion pit depth were listed in Table 2, and then the crack sprouting and expansion stage could be analyzed.

Table 2. Erosion pit depth at each corrosion age.

Corrosion life/a	0	10	30	50	80	100
Pit depth/mm	0	0.37	0.84	1.24	1.77	2.09

According to the traffic flow data of Humen Bridge health monitoring from 2004 to 2017, the crack expansion life of Humen Bridge top plate-U rib welded details was taken as an example, which showed an increasing trend year by year, among which the traffic growth curve of heavy vehicles (category four and five vehicles) was shown in Figure 18. It could be seen from the figure that the average annual growth rate of traffic volume for category four and category five vehicles from 2004 to 2017 was 11.18% and 12.01%. Then it could be projected that the annual traffic volume of heavy vehicles on Humen Bridge in 2022 would be 5,782,880 vehicles. The Humen Bridge was a six-lane bridge with an average annual traffic flow of 963,813 vehicles per lane. Only the heavier rear axle was counted when heavy vehicles pass through, so the annual number of vehicle loadings $N_{v,d}$ that account for fatigue damage was 963,813.

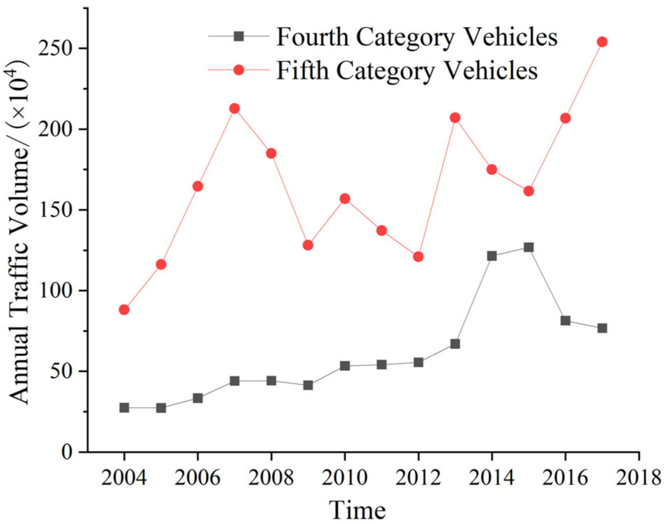

Figure 18. Humen Bridge heavy vehicle traffic volume change.

When the calculated number of fatigue crack propagation was N, the fatigue crack propagation life was

$$T_2 = \frac{N}{N_{v,d}} \tag{10}$$

The finite element model of the top plate-U rib welded details with a corrosion pit depth of 1.24 mm (i.e., corrosion life of 50 years) was taken as an example to calculate the total fatigue life of welding details. When the crack propagation reaches 1/2 of the thickness of the top plate, the number of crack propagation was 954.565, so the fatigue crack propagation life was calculated. Then the total fatigue life of welding details of the top plate-U rib with a corrosion life of 50 years was

$$T = T_1 + T_2 = 50 + 9.904 = 59.904a \tag{11}$$

5.2. Structural Design Impact Analysis

For top plate-U rib fatigue members on steel box girders in a marine corrosive environment, the corrosion of both the U rib web and the bottom plate was less than the top plate because the U rib was inside the steel box girder structure. This indicated that for the top plate-U rib welded fatigue details, the corrosion of the top plate was the dominant corrosion, and the top plate thickness was given priority in the design. On the basis of the above benchmark model member size, the shape, depth, and position of the pit were kept unchanged, and the top plate thickness changes were 12 mm, 14 mm, 18 mm, and 20 mm, respectively. The influence of the roof thickness changes on the structural details fatigue performance of the roof -U rib was analyzed.

Based on the above model and the method of implanting cracks, the crack expansion of the top plate-U rib welded details at each top plate thickness was simulated and analyzed. The crack tip stress intensity factor curve for the 0th extension step (crack implanted but not extended) at each top plate thickness was extracted and shown in Figure 19. As can be seen from the figure, with the top plate thickness increased, the 0th extension step crack tip stress intensity factor decreased. When the top plate thickness reached 18 mm, the minimum value of the stress intensity factor was less than the crack expansion threshold of 47 MPa·mm$^{1/2}$; when the top plate thickness reached 20 mm, the stress intensity factor was completely less than the crack expansion threshold. It indicated that the greater the top plate thickness, the smaller the driving force for the fatigue crack propagation of the top plate-U rib welded details, and the less likely the crack is to crack.

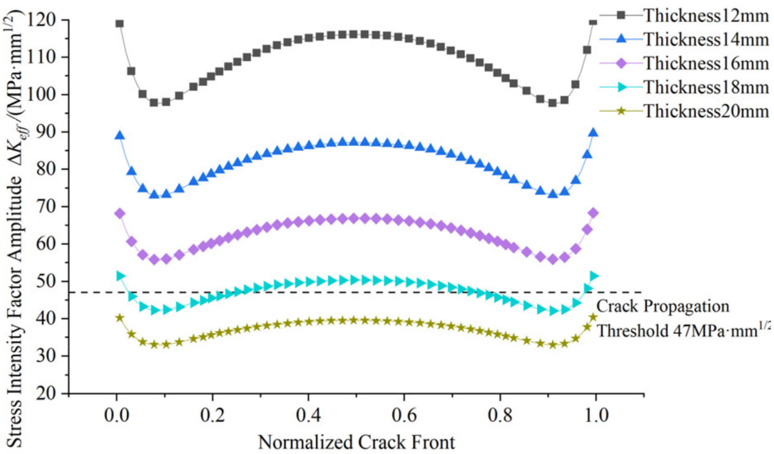

Figure 19. Crack tip stress intensity factor curve at the 0th extension step for different top plate thicknesses.

To study the influence of the top plate thickness on the crack extension life, the threshold value of 1 MPa·m$^{1/2}$ was reduced to 32 MPa·mm$^{1/2}$ under the premise of ensuring smooth crack extension, then the crack front stress intensity factor was less than the original threshold value of the crack can be smoothly cracked. As the thickness of the top plate is different, the critical damage value is half of the top plate thickness, leading to the destruction of the top plate-U rib welded details damage threshold value being different, so the impact of crack expansion average life (fatigue life at the critical point divided by the critical value, that is, the average life of crack expansion 1 mm) on the plate thickness is used to determine.

The fatigue life for different top plate thicknesses is shown in Figure 20, from which it could be seen that the fatigue crack expansion rate decreased significantly as the plate thickness increased. As the plate thickness increased from 12 mm to 14, 16, 18, and 20 mm, the fatigue life at each plate thickness critical point increased by 161.7%, 496.1%, 1316.6%, and 2956.4%, respectively, and the average crack extension life increased from 336,300 cycles/mm to 727,500 cycles/mm, 1,412,100 cycles/mm, 2,923,100 cycles/mm and 5,586,800 cycles/mm, a maximum increase of 1560.8%. This indicated that the effect of top plate thickness on the crack extension life of top plate-U rib fatigue members was significant.

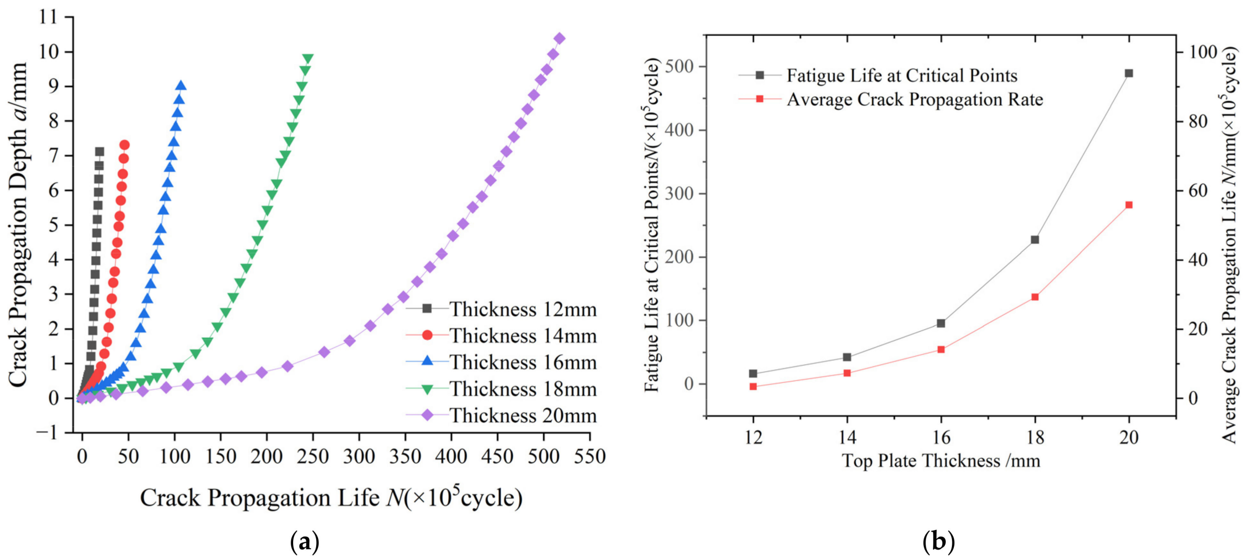

Figure 20. Fatigue life and average life of crack extension for different top plate thickness: (**a**) Fatigue life for different top plate thicknesses; (**b**) Fatigue life and average life of crack extension at critical point.

6. Conclusions

This paper was based on fracture mechanics of steel box beam welded details fatigue performance analysis method, through the finite element analysis software ABAQUS and FRANC3D, the top plate-U rib welded corrosion fatigue numerical simulation analysis methods were established to explore the action of welding details of the stress intensity factor and crack expansion in the marine corrosive environment and fatigue load coupled. On this basis, the crack growth life and the total fatigue life of welding details were explored, and the evaluation model of welding details corrosion fatigue life of top plate-U rib was established, and then the fatigue life under different roof thicknesses was explored. The above results showed that:

Firstly, for the uncorroded model, with the increase of crack propagation depth, the shape ratio of the crack increases rapidly to the maximum value and then decreases linearly, and the maximum value is about 0.82; for the corrosion model, when the crack front does not cross the boundary point, with the increase of the crack propagation depth, the shape ratio of the crack increases rapidly to the maximum value and then decreases, and the maximum value is about 0.70. When the crack front edge crosses the boundary point, the shape ratio decline rate slows down and decreases in a near-straight line. The decline rate is smaller than that of the uncorroded model, and it will intersect with the uncorroded model curve when the crack expands to 11 mm.

Secondly, the calculated corrosion life was 50 years, the corrosion depth was 1.24 mm, the top plate-U-rib welded detail finite element model was used as an example to calculate the total fatigue life of the welding details, the stress intensity factor was symmetrically distributed along the crack front. With the crack expansion step increased, the corresponding stress intensity factor amplitude also increased. When the crack crossed the corrosion pit, the stress intensity factor amplitudes at both ends of the crack front surged to 1.49 times the original amplitudes, with a small increase near the midpoint. When the crack depth extended to the half thickness of the top plate, the number of crack extensions was 954.565 and the total fatigue life of the top plate-U rib welded detail is $T = T_1 + T_2 = 50 + 9.904 = 59.904a$.

Thirdly, as the top plate thickness increased, the fatigue crack expansion rate decreased significantly. When the plate thickness increased from 12 mm to 20 mm, the fatigue life at each plate thickness critical point increased by 2956.4%; the average crack expansion life increased from 336,300 cycles/mm to 558,800 cycles/mm, an increase of 1560.8%. This indicated that the effect of top plate thickness on the crack extension life of the top plate-U rib fatigue members was significant.

Author Contributions: Methodology, Q.C.; Investigation, Q.C.; Project administration, Z.Y.; Validation, Z.Y.; Software, H.C.; Writing—original draft, D.L.; Writing—review & editing, M.L., Q.Z. and B.Z.; Funding acquisition, Q.Z. All authors have read and agreed to the published version of the manuscript.

Funding: This research was funded by the Research and Development Plan in key areas of Guangdong Province (2019B111106002).

Data Availability Statement: Data sharing not applicable.

Conflicts of Interest: The authors declare no conflict of interest.

References

1. Kayser, J.R.; Nowak, A.S. Reliability of corroded steel girder bridges. *Struct. Saf.* **1989**, *6*, 53–63. [CrossRef]
2. Cui, C.; Bu, Y.; Zhang, Q.; Li, L. Fatigue life evaluation of orthotropic steel bridge decks using the hot-spot stress method. *China Bridge Constr.* **2014**, *44*, 62–67.
3. Hobbacher, A.F. Recommendations for fatigue design of welded joints and components. In *Welding Research Council Bulletin*; (TN.520); Springer: Berlin/Heidelrberg, Germany, 2009.
4. Zhang, Q.; Cui, C.; Bu, Y.; Li, Q. Fatigue characteristics of orthotropic steel bridge deck of Hong Kong-Zhuhai-Macao bridge. *China Civ. Eng. J.* **2014**, *47*, 110–119. [CrossRef]
5. Meng, F. Ultimate Strength of Stiffened Plate Structures with Pitting Damage. Ph.D. Thesis, China Dalian University of Technology, Dalian, China, 2014.
6. Zhong, H. Typical diseases and research on long-span steel box girder suspension bridges. *China Sichuan Build. Mater.* **2017**, *43*, 2. [CrossRef]
7. Zhong, X. Study on crack disease analysis and treatment scheme of steel box girder of a highway bridge. *China Road Traffic Technol. Appl. Technol. Ed.* **2018**, *14*, 249–2524.
8. Zhou, S.; Shili, Y.; Qianhui, P.; Yong, Z. Fatigue Performance of Orthotropic Steel Decks in Long-Span Cable-Stayed Steel-Box Girder Railway Bridges. *J. Bridge Eng.* **2019**, *24*, 04019035. [CrossRef]
9. Wei, X.; Jie, Z.; Liao, X.; Xiao, L.; Qiang, S. Research progress on corrosion fatigue of welded joints of steel structure bridges. *China Steel Struct.* **2019**, *5*, 108–112. [CrossRef]
10. Zhang, J. Study on the Compressive Stability Bearing Capacity and Calculation Method of Stiffened Plate. Master's thesis, China Fuzhou University, Fuzhou, China, 2020.
11. Zhao, Q.; Yang, M.; Zhai, Z.; Wang, J. Numerical simulation of local stability of U-rib stiffened plate under compression. *China J. Archit. Sci. Eng.* **2017**, *34*, 32–40. [CrossRef]
12. Zhao, Q.; Zhai, S.; Chen, B.; Chen, Y.; Peng, Y. Experimental study on local stability of U-shaped rib stiffened plate. *China J. Build. Struct.* **2017**, *38*, 156–163. [CrossRef]
13. Zhao, Q.; Zhang, J.; Lin, C. Research on calculation method of local stability of U-rib stiffened plate under compression. *China J. Ningxia Univ. Nat. Sci. Ed.* **2020**, *41*, 252–261. [CrossRef]
14. *BS7910*; Guide on method for assessing the acceptability of flaws in metallic structures. British Standard Institution: London, UK, 2013.
15. *GB/T 15957-1995*; Corrosivity Classification of Atmospheric. Environment. Technical Supervision Bureau: Beijing, China, 1995.
16. Wang, X.; Wang, P.; Sun, Y.; Lian, B. Corrosion Resistance of Q235 Steel in Simulated Marine Atmospheric Environment. *Surf. Technol.* **2015**, *44*, 8. [CrossRef]
17. Liang, C.; Hou, W. Atmospheric Corrosion Prediction of Steel. *Chin. J. Corros. Prot.* **2006**, *26*, 129–135. [CrossRef]
18. *GB/T 1591-2018*; High strength low alloy structural steels. China National Standardization Administration Committee: Beijing, China, 2018.
19. *JTG D64-2015*; Specifications for Design of Highway Steel Bridge. Ministry of Transport: Beijing, China, 2015.

20. Suresh, S. *Fatigue of Materials*; Cambridge University Press: New York, NY, USA, 1998.
21. Forman, R.G.; Kearney, V.; Engle, R. Numerical analysis of crack propagation in cyclic-loaded structures. *J. Basic Eng.* **1967**, *89*, 459–463. [CrossRef]
22. Li, H. Investigation on Fracture Toughness and Crack Growth Mechanism of High-Strength Steels. Ph.D. Thesis, University of Science and Technology of China, Hefei, China, 2019.